MIXED MODE FRACTURE IN CONCRETE AND MASONRY

J. Alfaiate[1], L. J. Sluys[2] & E. B. Pires[1]

[1]Dept. Eng. Civil and ICIST, Instituto Superior Técnico, Lisboa, Portugal

[2]Dept. of Civil Eng. and Geosciences, Delft University of Technology, Delft, The Netherlands

ABSTRACT

In this paper, the finite element method is used to study mixed mode crack propagation in concrete and masonry. A discrete approach is adopted: cracks are allowed to evolve along discontinuity surfaces, called fictitious cracks. These discontinuities are modelled using: i) interface elements, in which case a numerical algorithm is adopted which avoids the need to remesh and ii) embedding discontinuities, according to a *discrete strong embedded discontinuity approach*. The effect of shear stresses which develop at the discontinuity surfaces is analysed. For this purpose: i) different values for mode-II fracture energy and cohesion are considered and ii) different softening criteria, both isotropic and non-isotropic, are adopted for the evolution of the limit surfaces in the discontinuity's stress vector space. It is found that the amount of shear stresses present in the discontinuity is the factor which influences most significantly the structural behaviour of both concrete and masonry.

1 INTRODUCTION

In this paper, Hillerborg's discrete approach is adopted to study mixed-mode crack propagation on concrete and masonry. Cracks are allowed to evolve along discontinuity surfaces, called fictitious cracks. Thus, microcracking is localized on an internal boundary with initial zero width, which eventually evolves into a stress free crack. In the past, the discrete approach has been modelled by means of interface elements, introduced along interelement boundaries. A numerical algorithm, presented in Alfaiate et al. [1], is adopted, both for prescribed and non-prescribed cracking, without the need to remesh. According to the work presented in Alfaiate and Sluys [2], these localized surfaces can be modelled within the framework of a discrete approach by means of embedding discontinuities into the finite elements. This embedded discontinuity approach is also followed here.

Cracks are allowed to open according to a mode-I fracture criterion and crack growth is modelled under mixed-mode conditions using either plasticity or damage laws. Both aggregate interlock and shear fracture are taken into account; the corresponding dissipated energy depends upon a mode-II parameter, denoted by G_F^{II}, as well as on a limit surface defined in the discontinuity's stress vector space. In the numerical tests performed on notched concrete specimens, different models are adopted in order to evaluate the differences between mixed-mode and pure mode-I analyses. In particular, the effect of shear stresses which develop at the discontinuity surfaces is analysed. For this purpose: i) different values for G_F^{II} and cohesion are considered and ii) different softening criteria, both isotropic and non-isotropic, are adopted for the evolution of the limit surfaces. It is found that the structural response in mixed-mode does not depend significantly on the cohesion or G_F^{II}; conversely, the adoption of different softening criteria gives rise to different post-peak load-displacement curves. In particular, non-isotropic softening rules which allow for higher shear stresses to develop at crack faces approximate better the post-peak regime which was experimentally observed.

This analysis is further extended to a masonry wall. The brick-mortar joints are modelled by interface elements and the limit surfaces mentioned above are used to evaluate the dissipation of

energy under slippage. Interestingly, it is found that different limit surfaces and softening criteria can lead to different failure mechanisms as well as different ultimate loads, which is verified experimentally (Alfaiate and de Almeida [3]).

2 MATERIAL MODELS

Two different zones within the material can be distinguished in the adopted model: i) the bulk, for which an elastic or plastic relationship is assumed and: ii) the fracture zones, which are modelled by a discrete approach. In a discrete approach the fracture zone, where microcracking occurs, is assumed to localise into surfaces of discontinuity. It is assumed that crack initiation occurs according to mode-I fracture: when the maximum principal stress reaches the tensile strength of the material, f_t, a fictitious crack is introduced perpendicularly to the maximum principal stress direction. In this section, two different types of discrete constitutive models are considered for the fracture zones: i) damage models and ii) plasticity models.

2.1 Damage models

Two damage models are considered to describe the constitutive response at a discontinuity surface. In the first model isotropic damage is adopted, whereas a non-isotropic response is obtained with the second model. The damage model with isotropic softening is derived from a thermodynamical framework through the definition of the free energy per unit area, Ψ, given by (Alfaiate et al. [4]):

$$\Psi(\mathbf{w},d) = (1-d)\Psi_0(\mathbf{w}) = \frac{1}{2}\ (1-d)\ \mathbf{w}\cdot\mathbf{D}_{\Gamma_d}^{el}\cdot\mathbf{w} \tag{1}$$

where $\mathbf{w}$ is the displacement jump vector at the discontinuity surface Γ_d, $\mathbf{D}_{\Gamma_d}^{el}$ is a second order elastic constitutive tensor and d is a scalar damage parameter. Standard thermodynamic arguments lead to the state equation

$$\mathbf{t} = \frac{\partial\Psi}{\partial\mathbf{w}} = (1-d)\ \mathbf{D}_{\Gamma_d}^{el}\cdot\mathbf{w}. \tag{2}$$

Since the elastic free energy per unit area is positive, the rate of d cannot be negative, i.e., $\dot{d}\geq 0$. An exponential softening evolution law for the damage parameter d is adopted.

The non-isotropic damage model consists of a 2D version of the model introduced in Wells and Sluys [5]. A loading function is defined as:

$$f(w_n,\kappa) = w_n - \kappa \tag{3}$$

where the internal variable κ is taken as the maximum normal relative displacement reached ($\kappa=\max(w_n)$, $\dot{\kappa}\geq 0$). The total $\mathbf{t}$-$\mathbf{w}$ relationship is given by:

$$t_n = f_{t0}\exp\left(-\frac{f_{t0}}{G_F}\kappa\right),\quad t_s = D_{s0}\exp(-h_s\kappa)w_s, \tag{4}$$

where t_n, t_s, w_n and w_s are the normal and tangential components of vectors $\mathbf{t}$ and $\mathbf{w}$, respectively, D_{s0} is the initial shear stiffness at crack initiation, $h_s = \ln(D_{s\kappa}/D_{s0})$ and $D_{s\kappa}$ is the shear stiffness which is adopted for an advanced state of damage.

2.2 Plasticity model

A plasticity model is also adopted to model the fracture behaviour of the fracture zones. In this model, a yield surface is defined in the discontinuity's stress vector space $\{t_n, t_s\}$, such that both tensile mode-I cracking and a modified friction Coulomb envelope are taken into account. In fig. 1-a) four adopted yield surfaces are shown. The limit surface f_1 is a tensile cap corresponding to mode-I crack evolution. Surface f_2 represents the Mohr-Coulomb friction law. The curved surfaces f_3 and f_4 correspond to modified Coulomb friction laws in which the shear stresses remain bounded,

with the limitation on the shear strength being more pronounced for surface f_4. Both the tensile strength f_t and the cohesion c soften according to exponential flow rules (Alfaiate et al. [3,4]). Both non-isotropic and isotropic softening criteria are adopted. In the former case, surfaces f_1 and f_2 are used and the shear stress at the intersection of both surfaces is kept constant as depicted in fig. 1-b). An isotropic softening criterion is also adopted; in this case, the limit surfaces contract towards the origin such that the tensile strength and the cohesion decrease proportionally the same amount, as depicted in fig 1-a) for surface f_4.
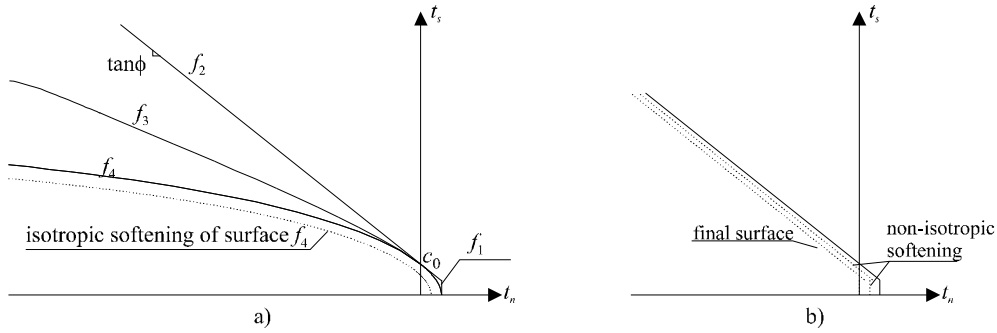

Figure 1: adopted yield surfaces in the discontinuity's stress vector space

3 NUMERICAL RESULTS

3.1 Concrete

The concrete tests consist of two single edge-notched beams submitted to shear. The first beam was experimentally tested by Arrea and Ingraffea [6], whereas the second beam, with different dimensions but subjected to similar boundary conditions, was tested by Schlangen [7]. The first beam is analysed with interface elements, adopting the algorithm introduced in Alfaiate et al. [1], in which the properties of the fictitious cracks are projected on the directions of the interelement boundaries such that no remeshing is necessary. Four different numerical tests are presented. In Table 1 the parameters and softening criteria adopted are shown. In all tests the plasticity model described in section 2.2 is adopted. The first test corresponds to pure mode-I cracking since no shear stresses are allowed in the fictitious crack. In the last three tests, data is chosen in order to show the importance of the shear behaviour in the fictitious crack. In the second test a very high G_F^{II}/G_F relation is adopted ($G_F^{II}/G_F = 100$), where G_F and G_F^{II} are the fracture energies in mode-I and mode-II fracture, respectively. In the third test a cohesion value which is twice the value of the tensile strength is adopted, and in the fourth test a non-isotropic softening criterion is considered. In fig. 2-a) the deformed mesh obtained form test No.2 is shown. In fig. 2-b) the P-CMSD (load - crack mouth sliding displacement) relations are presented. The experimental results lie in the shadowed region of fig. 2-b). From fig. 2-b) it is clear that, according to the model and data proposed, small differences are observed between pure mode-I and mixed-mode analysis for the peak load. From Test Nº4, it is found that the post-peak response is stiffer than the other two. An explanation for this is advanced below. The second beam is analysed using embedded discontinuities.

Test No.	E (GPa)	f_t (MPa)	c_0/f_t	G_F (N/mm)	G_F^{II}/G_F	ϕ friction	softening criterion
1	24.8	2.8	0	0.1	0		
2	24.8	2.8	1	0.1	100	30°	isotropic
3	24.8	2.8	2	0.1	1	30°	isotropic
4	24.8	2.8	1	0.1	1	30°	non-isotropic

Table 1: Material parameters and softening criteria adopted in the first numerical tests.

The material properties adopted are: Young's modulus $E = 35$ GPa; Poisson's ratio $\nu = 0.15$; tensile strength $f_t = 2.8$ MPa; fracture energy $G_F = 0.1$ MPa·mm. In these numerical tests three different constitutive models are adopted:

1. the isotropic damage model described in 2.1.1, with $c_0 = f_{t0}$;
2. the non-isotropic damage model described in 2.1.2, with $D_{s0} = 10^3$ MPa/mm;
3. the plasticity model described in section 2.2; in this case, two different tests are performed:
   i) $c_0 = f_{t0} = 2.8$ MPa, $G_F^{II} = G_F = 0.1$ N/mm and ii) $c_0/f_{t0} = G_F^{II}/G_F = 2$.
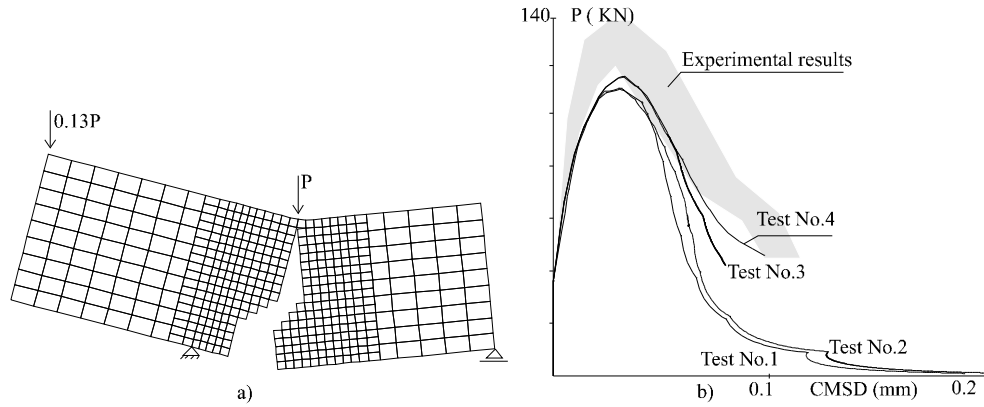

Figure 2: a) deformed mesh (test No.2) and b) load-CMSD curves

The load-CMSD curves are shown in fig. 3. It is clear that the result obtained with the non-isotropic damage model, presented in fig. 3-b), is significantly different from the others: in this case, the higher shear stresses allowed in the discontinuity give rise to a stiffer softening response which is closer to the experimental one. In fig. 4 the relations between the shear stresses at the notch and the CMSD (τ_{notch}-CMSD curves) obtained with the different models are presented. In this figure it can be confirmed that the non-isotropic damage model gives rise to higher shear stresses than the other models.

3.2 Masonry

A wall with an opening is numerically analysed with the plasticity model and the four limit surfaces, f_1, f_2, f_3 and f_4, defined in section 2.2. Cracking of the bricks is modelled using the numerical algorithm introduced in Alfaiate et al. [1] and crushing is modelled by means of a continuum plasticity model. In the first test, surfaces f_1 and f_2 are adopted for the mortar interfaces and it is verified that the numerical peak load is far beyond the experimental value, as shown in fig. 5. The decrease of shear strength with high compressive stresses, introduced by surfaces f_3 and f_4, allow for a better approximation of the experimentally obtained peak loads. The higher peak load value corre-

sponds to a failure mechanism which involves the formation of plastic hinges, induced by crushing of the bricks. The lowest peak load corresponds to the formation of a different failure mechanism, where the amount of slippage at the mortar interfaces is such that no crushing occurs in the bricks. These different mechanisms, which were also observed experimentally, are depicted in fig. 6, as well as the corresponding deformed meshes.
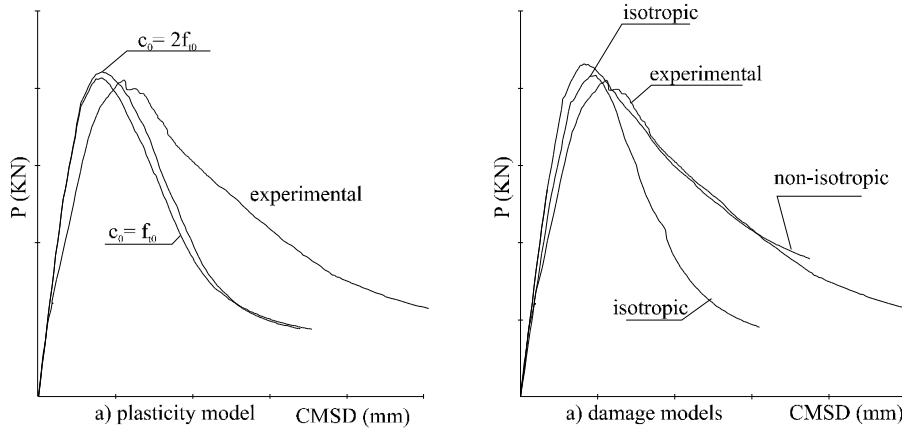

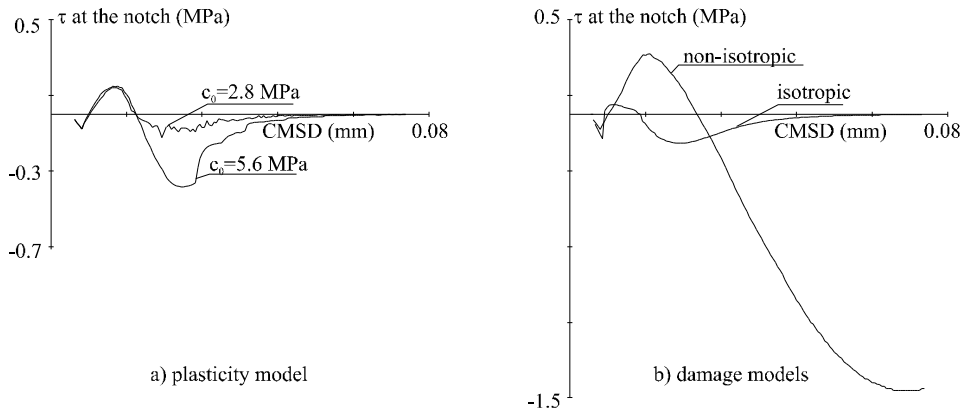Figure 3: load-CMSD curves obtained with embedded discontinuities

Figure 4: τ_{notch}-CMSD curves

4 CONCLUSIONS

From all tests analysed, it is verified that the amount of shear stresses present at the discontinuities is the most important factor in mixed-mode fracture of both concrete and masonry. In concrete, it is found that larger shear stresses lead to both a stiffer post peak response and to a better approximation of the softening regime experimentally observed; it is also found that mixed-mode fracture does not depend significantly either on the mode-II fracture energy or on the cohesion. In masonry, if slippage at the mortar interfaces is allowed to fully develop, the limitation of shear stresses under high compressive stresses may lead to a smaller peak load as well as different failure mechanisms, which was also confirmed experimentally.
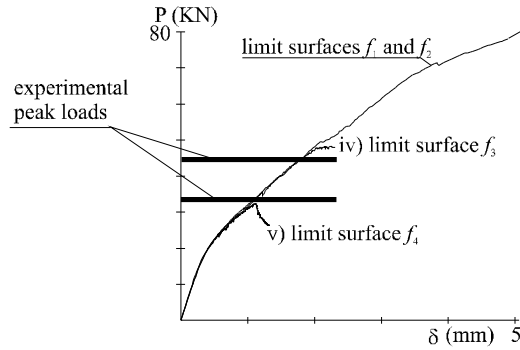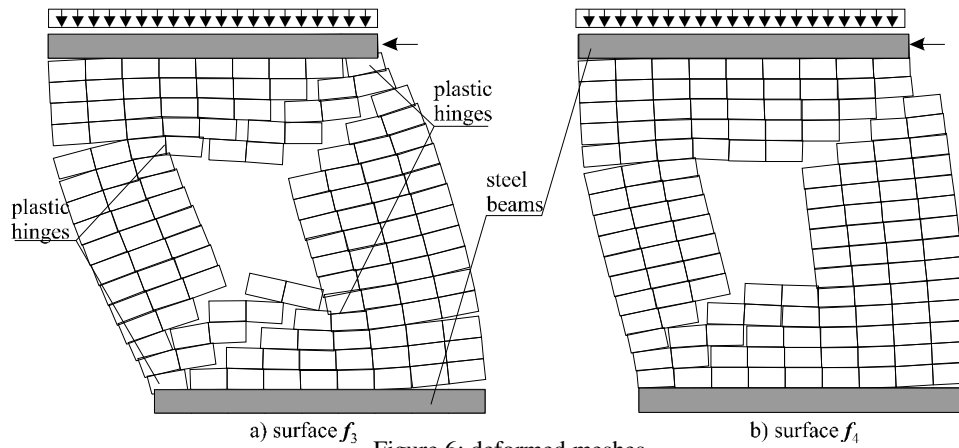
Figure 5: load-displacement curves

a) surface f_3 b) surface f_4

Figure 6: deformed meshes

REFERENCES

[1] Alfaiate J., Pires E. B., and Martins J. A. C., A Finite Element Analysis of Non-Prescribed Crack Propagation in Concrete, Computers & Structures, 63, 1, 17-26, 1997.

[2] Alfaiate J., and Sluys L. J., A discrete strong embedded discontinuity approach, in Victor C. Li, Christopher K.Y. Leung, Kasper Willam and Sarah Billington eds. Fracture Mechanics of Concrete and Concrete Structures - Framcos 5. Proc. 5th Int. Conf., Vail Colorado, USA, 2004.

[3] Alfaiate J., de Almeida J., Modelling discrete cracking on masonry walls, Masonry International, 2004, *in press*.

[4] Alfaiate J., Wells G. N. and Sluys L. J., On the use of embedded discontinuity elements with crack path continuity for mode I and mixed mode fracture, Engineering Fracture Mechanics, 69(6), 661-686, 2001.

[5] Wells G. N., Sluys L. J., Three-dimensional embedded discontinuity model for brittle fracture, International Journal of Solids and Structures, 38(5), 897—13, 2001.

[6] Arrea M. and Ingraffea A., Mixed mode crack propagation in mortar and concrete, Dept. of Structural Engineering, Cornell University, USA, 1982.

[7] Schlangen E., Experimental and numerical analysis of fracture processes in concrete. Ph.D. thesis, Delft University of Technology, 1993.